Tellus (1998), 50B, 224–242
Printed in UK – all rights reserved

TELLUS
ISSN 0280–6495

Simulation of global sulfate distribution and the influence on effective cloud drop radii with a coupled photochemistry-sulfur cycle model

By GEERT-JAN ROELOFS,* JOS LELIEVELD AND LAURENS GANZEVELD, *Institute for Marine and Atmospheric Research Utrecht (IMAU), Prinetonplein 5, 3584 CC Utrecht, The Netherlands*

(Manuscript received 30 June 1997; in final form 6 February 1998)

ABSTRACT

A sulfur cycle model is coupled to a global chemistry-climate model. The simulated surface sulfate concentrations are generally within a factor of 2 of observed concentrations, and display a realistic seasonality for most background locations. However, the model tends to underestimate sulfate and overestimate surface SO_2 at relatively polluted locations. A possible explanation for this is that additional oxidation reactions not considered in the model, may be important. Calculated tropospheric sulfate column abundances exceed those of previous studies, which is predominantly associated with a less efficient nucleation scavenging in wet convective updrafts. Through the simultaneous calculation of the sulfur cycle and tropospheric photochemistry, simulated H_2O_2 and SO_2 concentrations are strongly linked, especially in polluted areas. The coupled model simulates a stronger oxidant limitation and, consequently, a smaller contribution to sulfate formation by H_2O_2 oxidation of SO_2 when compared to sulfur cycle models that use monthly averaged oxidant distributions as input. In the polluted NH, the differences in calculated sulfate columns are largest in winter and relatively small in summer. Therefore, the coupling between the sulfur cycle and the oxidant chemistry is expected to have a minor impact on the calculation of the indirect and direct radiative forcing by sulfate. An empirical relation between sulfate concentration and cloud drop number concentration, derived from cloud measurements at Grean Dun Fell (UK), is applied to the simulated cloud and sulfate fields to derive distributions of effective could drop radii. Additionally, a relation between wind speed and cloud drop number concentration is applied over marine regions to account for the effect of seasalt aerosol on cloud formation when sulfate concentrations are relatively low. Calculated droplet radii are systematically underestimated by about 10–20% in the NH compared to satellite derived values, but they agree relatively well in the SH.

1. Introduction

In recent years, it has become apparent that the anthropogenic aerosol perturbation of the lower troposphere affects climate with a magnitude that may be comparable, although with opposite sign, to that of the greenhouse gases, at least in the northern hemisphere (IPCC, 1996). Firstly, the increased aerosol load in the atmosphere reflects more incident short-wave radiation back to space (the "direct" effect) (Charlson et al., 1992; Kiehl and Briegleb, 1993). Secondly, increasing aerosol number concentrations influence the cloud microphysics, thus reducing the cloud droplet effective radii and increasing the cloud albedo. Further, cloud lifetimes may increase due to a decrease in the precipitation formation efficiency (these influences constitute the "indirect" effect) (Twomey,

* Corresponding author.

1974; Albrecht, 1989; Jones et al., 1994; Boucher and Lohmann, 1995). The aerosol climate forcing involves mainly aerosols in the sub-micrometer and micrometer size range, with a chemical composition dominated by sulfates. Globally, anthropogenic sulfur sources exceed natural sources by a factor of 3 to 4. Emissions from fossil fuel burning predominate, and about 90% of the anthropogenic sources are located in the NH (Langner and Rodhe, 1991).

The atmospheric lifetime of sulfate is of the order of a few days. Compared to the long-lived greenhouse gases, aerosol concentrations are therefore highly variable in space and time. Three-dimensional chemistry/transport models that simulate the sources, transports, transformations, and sinks of sulfur-containing species are important tools for the study of the global distribution of sulfate. Langner and Rodhe (1991) used the 3D tropospheric model MOGUNTIA (Crutzen and Zimmerman, 1991) which is driven by monthly averaged wind fields. Recently, global sulfur cycle models have been developed by Chin et al. (1996), Feichter et al. (1996), and Pham et al. (1995).

The chemistry and microphysics of aerosols and clouds play an important role in the indirect aerosol-climate effect. The activation and growth of cloud drops, as well as cloud chemistry, are directly and non-linearly influenced by the aerosol number concentration, size distribution and chemical composition (Pruppacher and Klett, 1978). Accurate, yet computationally efficient parametrizations of the processes that couple aerosol and cloud microphysics are needed for global climate models. Results of such an approach are presented by Ghan et al. (1997), and indicate a strong sensitivity of the droplet number concentration to the vertical resolution of the model.

Jones et al. (1994) used an empirical relation between aerosol concentrations and cloud drop number concentrations (CDNC) as a simplified microphysical parametrization. They applied this relation to global sulfate distributions calculated by Langner and Rodhe (1991) and GCM-calculated cloud liquid water distributions, and calculated an indirect climate forcing by changing cloud albedo of $-1.3\ \mathrm{W\,m^{-2}}$. Using similar approaches, Boucher and Lohmann (1995) and Feichter et al. (1997) estimated a global indirect forcing of -1.0 and $-0.75\ \mathrm{W\,m^{-2}}$, respectively. The related large uncertainty is reflected in IPCC (1996), reporting a range of 0 to $-1.5\ \mathrm{W\,m^{-2}}$. Boucher and Lohmann (1995) demonstrated the sensitivity of the forcing estimate to the specific sulfate-CDNC relation used for the calculation. Recently, Chuang et al. (1997) presented an approach based on the condensation and chemical formation of anthropogenic sulfate on a pre-existing aerosol size distribution. They calculated an indirect effect between 0.6 and $-1.6\ \mathrm{W\,m^{-2}}$. Lohmann and Feichter (1997) studied the indirect effect due to an increasing cloud lifetime by changes in the precipitation efficiency caused by enhanced sulfate concentrations. They concluded that the uncertainties linked to the indirect effect on radiative forcing may be much higher than previously suggested.

In this work we analyze the representativeness of a sulfate-CDNC relation that is obtained from measurements during the Great Dun Fell experiment in 1993 (Choularton et al., 1997). Firstly, we present an updated version of the global sulfur model of Feichter et al. (1996) and Lelieveld et al. (1997). The chemistry scheme of the model, which is coupled to the general circulation model ECHAM, considers the background tropospheric CH_4–CH–HO_x–NO_x chemistry and the sulfur cycle as a coupled system, and calculates concentrations of all relevant chemical species simultaneously and interactively. In the previous model (Feichter et al., 1996) the oxidation of SO_2 was based on prescribed oxidant fields (OH, O_3, H_2O_2) calculated off-line by a chemistry-climate model. This approach neglects the strong coupling of H_2O_2 and SO_2, which can be especially important in the winter HN when photochemical production of H_2O_2 is relatively low. Further, the sulfur scheme incorporates a detailed dry deposition scheme (Ganzeveld et al., 1998) that is directly coupled to the ECHAM boundary layer meteorology. The model is described in Section 2. In Section 3, we evaluate the model performance by comparing calculated SO_2 and sulfate surface concentrations with observations and discuss budgets and global distributions. In Section 4, we compare results of the coupled model with two simulations that use monthly averaged oxidant fields calculated with and without considering the sulfur cycle, and discuss the effect of the coupling of the photochemistry and the sulfur schemes on the sulfate burden and on radiative forcing calculations. In section 5, we present the calculated effective droplet radii that are derived from the

cloud fields simulated by the climate model, and compare these with effective droplet radii retrieved from satellite measurements and with results based on similar parameterizations from Jones et al. (1994) and Boucher and Lohmann (1995). Section 6 presents the conclusions.

2. Model description

2.1. The general circulation model ECHAM

The ECHAM spectral general circulation model (version 4) is based on the ECMWF numerical weather prediction model (Roeckner et al., 1996). Vorticity, divergence, temperature, surface pressure, humidity, and cloud water are prognostic variables. Radiation, large scale and convective cloud formation and precipitation are calculated by the model, as well as explicit boundary layer mixing process. Land surface processes are described by a 5-layer heat conductivity soil model and by a hydrological model to determine evaporation and runoff. Sea surface temperatures are prescribed. In the T21 mode, which is used in this study, the horizontal resolution is approximately $5.6^\circ \times 5.6^\circ$ and the time resolution is 2400 s. The model has 19 vertical layers in a hybrid σ-p-coordinate system, from the surface of 10 hPa. Average pressure levels relevant for the troposphere and lower stratosphere are 990, 970, 950, 900, 840, 760, 670, 580, 490, 400, 320, 250, 190, 140, 100 and 75 hPa, referring to approximate mid-layer altitudes of 0.03, 0.14, 0.38, 0.78, 1.4, 2.1, 3.1, 4.2, 5.6, 7.0, 8.6, 10.2, 11.9, 13.8, 15.9 and 18.0 km above the surface, respectively. ECHAM4 distinguishes between large scale and convective clouds. The large scale cloud scheme is based on the work of Sundqvist (1978) and Roeckner et al. (1991), and calculates condensation of water vapor, evaporation of cloud water, formation of precipitation by coalescence of cloud droplets and sedimentation of ice crystals, and the evaporation of precipitation in unsaturated air. Convective clouds are represented by a bulk model and include updraft and downdraft mass fluxes, following the mass flux scheme of Tiedtke (1989). The scheme distinguishes between penetrative convection, shallow convection and mid-level convection. Additional vertical transports are included through parameterizations for vertical diffusion (Roeckner et al., 1996). Tracer transport is calculated using a semi-Lagrangian advection scheme (Rasch and Williamson, 1990). An elaborate description of ECHAM and the simulated climate can be found in Roeckner et al. (1995, 1996), Haskins et al. (1995), and Chen and Roeckner (1996, 1997).

2.2. The chemical model

The GCM is coupled to a tropospheric chemistry model, that considers background CH_4–CO–NO_x–HO_x chemistry, emissions of NO and CO, dry deposition of O_3, NO_2, HNO_3, and H_2O_2, and wet deposition of HNO_3 and H_2O_2. The coupled model realistically represents the seasonal variabilities of the O_3 photochemical production and of O_3 transport from the stratosphere. Calculated O_3 profiles and surface concentrations for remote tropical and mid-latitudinal sites agree well with observations (Roelofs and Lelieveld, 1995, 1997).

We have extended the model with a scheme describing the sulfur cycle. The model considers DMS and SO_2 in the gas phase and (particulate) sulfate. For a particular grid cell, the time rate of change of their concentrations is given by:

$$\frac{\mathrm{d\,DMS}}{\mathrm{d}t} = \left.\frac{\partial\,\mathrm{DMS}}{\partial t}\right|_{\mathrm{tr}} + \left.\frac{\partial\,\mathrm{DMS}}{\partial t}\right|_{\mathrm{em}} + \left.\frac{\partial\,\mathrm{DMS}}{\partial t}\right|_{\mathrm{ch}}, \tag{1}$$

$$\frac{\mathrm{d\,SO_2}}{\mathrm{d}t} = \left.\frac{\partial\,\mathrm{SO_2}}{\partial t}\right|_{\mathrm{tr}} + \left.\frac{\partial\,\mathrm{SO_2}}{\partial t}\right|_{\mathrm{em}} + \left.\frac{\partial\,\mathrm{SO_2}}{\partial t}\right|_{\mathrm{ch}} + \left.\frac{\partial\,\mathrm{SO_2}}{\partial t}\right|_{\mathrm{dd}} + \left.\frac{\partial\,\mathrm{SO_2}}{\partial t}\right|_{\mathrm{ev}}, \tag{2}$$

$$\frac{\mathrm{dSO_4}}{\mathrm{d}t} = \left.\frac{\partial\mathrm{SO_4}}{\partial t}\right|_{\mathrm{tr}} + \left.\frac{\partial\mathrm{SO_4}}{\partial t}\right|_{\mathrm{em}} + \left.\frac{\partial\mathrm{SO_4}}{\partial t}\right|_{\mathrm{ch}} + \left.\frac{\partial\mathrm{SO_4}}{\partial t}\right|_{\mathrm{dd}} + \left.\frac{\partial\mathrm{SO_4}}{\partial t}\right|_{\mathrm{nu}} + \left.\frac{\partial\mathrm{SO_4}}{\mathrm{d}t}\right|_{\mathrm{im}} + \left.\frac{\partial\mathrm{SO_4}}{\partial t}\right|_{\mathrm{ev}} \tag{3}$$

The subscripts tr, em, ch, dd, nu, im, and ev denote transport, emissions, gas and aqueous phase chemical processes, dry deposition, nucleation scavenging in clouds, impaction scavenging by precipitation, and evaporation of clouds and precipitation, respectively. We note that the coupling between the sulfur cycle and the tropospheric background chemistry does not significantly alter the concentrations of O_3 and OH compared to Roelofs and Lelieveld (1995) since the reactions

with SO_2 constitute minor sinks compared to other sinks. On the other hand, the concentration of H_2O_2 is strongly coupled to SO_2. The coupling results in a decrease of the H_2O_2 abundance, integrated over the troposphere between 30°–90°N, by 27% in January and 8% in July. Finally, the radiation code of the GCM uses default O_3 and aerosol distributions (Roeckner et al., 1996), so that the chemistry calculations do not affect the simulated meteorology.

2.3. *Emissions of DMS, SO_2, and sulfate*

Simulated global emissions of DMS are distributed according to Bates et al. (1992), with 15.5 Tg S yr^{-1} over the ocean and 1.1 Tg S yr^{-1} over land. The latitudinal oceanic DMS emissions were distributed within latitude bands using monthly pigment concentrations from the Coastal Zone Color Scanner (CZCS) (C. Benkovitz, personal communication). The volcanic contribution to natural SO_2 emissions is 7.8 Tg S yr^{-1} (Spiro et al., 1992). Sulfur releases from explosive eruptions have been neglected. Anthropogenic sulfur emissions considered in the model amount to 67 Tg S yr^{-1} and are distributed according to GEIA (Global Emissions Inventory Activity), version 1B.1 (E. C. Voldner, M. T. Scholtz, K. A. Davidson, Y.-F. Li and C. M. Benkovitz, 1 degree × 1 degree global SO_x and NO_x two-level emissions inventories resolved seasonally into emission vectors and point and area sources, manuscript in preparation; Benkovitz et al., 1996). The inventory refers to circa 1985 and includes a moderate seasonal resolution and two vertical levels, defined as surface (0 − 100 m, about 35% of the emitted sulfur) and elevated (above 100 m, about 65%). In our model, the surface layer has a thickness of approximately 60 m. We assume that the lower level emissions are equally distributed between the surface and 100 m altitude. Consequently, about 75% of the anthropogenic sulfur are emitted in the layer above the surface layer, i.e., between 60 and 220 m altitude. Following Langner and Rodhe (1991), we assume that 5% of anthropogenic sulfur emissions are released as sulfate. Anthropogenic sulfur emissions from biomass burning release an additional amount of 2.3 Tg S yr^{-1}, distributed according to Hao and Liu (1994). Total contemporary emissions of NO_x and CO are 36.5 Tg N yr^{-1} and 1900 CO Tg yr^{-1}, respectively (Roelofs and Lelieveld, 1995, 1997).

2.4. *Chemical reactions involving DMS < SO_2 and sulfate*

In the model, DMS reacts with NO_3 and OH which is directly followed by formation of SO_2. In the gas phase, SO_2 is oxidized by OH to sulfuric acid. The corresponding reaction rates in the model are from Atkinson et al. (1992). We assume that each sulfuric acid molecule is immediately transformed to NH_4HSO_4. The aqueous phase chemistry scheme considers dissolution of SO_2, O_3, HNO_3 and H_2O_2 in cloud or precipitation droplets, the dissociation of dissolved SO_2 and HNO_3, and the oxidation of S(IV) ($SO_2(aq) + HSO_3^- + SO_3^{2-}$) to sulfate by O_3 and H_2O_2. Mass transfer is calculated using the Froessling equation (Schwartz, 1986). Gas phase transport limitations are considered; interfacial and liquid phase transport limitations are found to be significant only under certain extreme conditions and are neglected in this study (Schwartz, 1988). All accommodation coefficients are assumed to be unity. Aqueous phase chemical reaction rates and the Henry Law coefficients are the same as in Roelofs (1992).

Following Boucher and Lohmann (1995), we assume that 60% of the particulate matter is taken up by nucleation scavenging during cloud formation. Concentration changes for gaseous SO_2, O_3, HNO_3, and H_2O_2, and liquid phase SO_4^{2-}, HSO_3^-, H_2O_2, NO_3^-, and H^+ are calculated interactively using an Eulerian backward Iterative (EBI) numerical chemistry scheme (Roelofs and Lelieveld, 1995). Additional input parameters for the scheme are LWC, pressure, and temperature, which are calculated by ECHAM4, and a representative cloud or rain drop size. Calculation of the cloud drop radius is analogous to that of the effective cloud drop radii that is described in Section 5. The LWC and drop radius in rain are calculated from the ECHAM4 precipitation rate using empirical relationships given in Mason (1971). Aqueous phase chemistry is assumed to take place in liquid hydrometeors only. Each mole of SO_4^{2-} that is produced in cloud or rain water is assumed to be associated with one mole of H^+ and one of NH_4^+, which allows for an explicit calculation of the pH. The precipitation formation

rate calculated by ECHAM4 determines the fraction of dissolved species transported from cloud water to rain water; the remainder is released to the gas phase at the end of the time step (Roelofs and Lelieveld, 1995). Precipitation is assumed to be ice for temperatures below 0°C, and liquid otherwise. Below-cloud scavenging of aerosols is calculated using the parametrization of Scott (1978). Release to the atmosphere of chemical species form rain is proportional to the precipitation evaporation in ECHAM4 (Roeckner et al., 1991).

2.5. *Dry deposition*

The parametrization for the dry deposition of O_3, NO_x, and HNO_3 is described in Ganzeveld and Lelieveld (1995). It derives aerodynamic and stomatal resistances directly from parameters calculated by ECHAM4. Dry deposition of SO_2 and sulfate is calculated according to the "big-leaf" and "multi-resistance" concepts (Hicks et al., 1987). The turbulent transfer and vegetation activity are computed by ECHAM4, supplemented with representative uptake rates for soil, water, and snow and ice on a global scale. Recent improvements of the deposition scheme include the use of a local surface roughness, and a more realistic representation of the leaf area index (LAI). Over snow and ice we assume an SO_2 dry deposition velocity of 0.1 cm s^{-1}. The SO_2 and sulfate dry deposition velocities calculated with a new scheme are generally smaller over land and larger over sea compared to the fixed dry deposition values used in the previous model (Feichter et al., 1996). For a detailed presentation of the dry deposition scheme and discussion of the results we refer to Ganzeveld et al. (1998).

3. Simulation of the global sulfate distribution and budget

3.1. *Comparison with surface concentration measurements*

The results presented in this section are averaged over three simulation years. Fig. 1 shows monthly averaged calculated and observed concentrations of sulfate for selected locations. The dotted lines illustrate the horizontal gradients of simulated concentrations. They refer to maximum and minimum concentrations at the grid boundaries, obtained from averaging grid cell concentrations with those in neighboring grid cells. Observed data, compiled by Chin et al. (1996), are from the EMEP Data Report (1988–1994), Shaw and Paur (1983), Li and Barrie (1993), Prospero et al. (1995), Galloway et al. (1993), Savoie et al. (1993, 1994), and Ayers et al. (1986, 1991). Calculated sulfate concentrations are significantly lower than measured for Europe and North America which are relatively polluted (Figs 1a–e). Furthermore, the model does not capture the relatively high sulfate concentrations in winter over Europe. Monthly averaged surface SO_2 is overestimated by about a factor of 2, as shown in Fig. 2 (observed data from the EMEP Data Report, 1988–1994; Shaw and Paur, 1983; Barrie and Bottenheim, 1990). However, the SO_2 seasonality is reproduced relatively well. A possible explanation for the discrepancy between modelled and observed SO_2 and sulfate concentrations is an underestimation of the oxidation rate of SO_2. It has been suggested that additional heterogeneous oxidation mechanisms of SO_2 that are not included in the model, e.g., on the surface of atmospheric aerosols, may account for part of the discrepancies (Feichter et al., 1996; Dentener et al., 1996; Kasibhatla et al., 1997). Also, the assumption of a monodisperse drop size distribution (the bulk approach) may underestimate the SO_2 oxidation (Roelofs, 1993). Further, as previously observed in a study of NO_x (Roelofs and Lelieveld, 1995), it is possible that mixing processes within the boundary layer or between the boundary layer and the free troposphere are somewhat suppressed in the model. This is also indicated by results from a ^{222}Rn tracer study with ECHAM, showing anomalously high surface ^{222}Rn concentrations compared to observations and to other models (Jacob et al., 1997). Finally, we note that the simulated emissions refer to circa 1985, whereas the observations were performed during periods between 2 and 20 years, not always including 1985 (Chin et al., 1996). For this reason the simulations may not be entirely representative for the observation periods for the individual sites. Nevertheless, the seasonality of sulfate surface concentrations is reproduced relatively well at remote sites except for Heimaey, Samoa and Cape Grim (Fig. 1f–o). Simulated concentrations are generally within a factor of 2 of the observations.

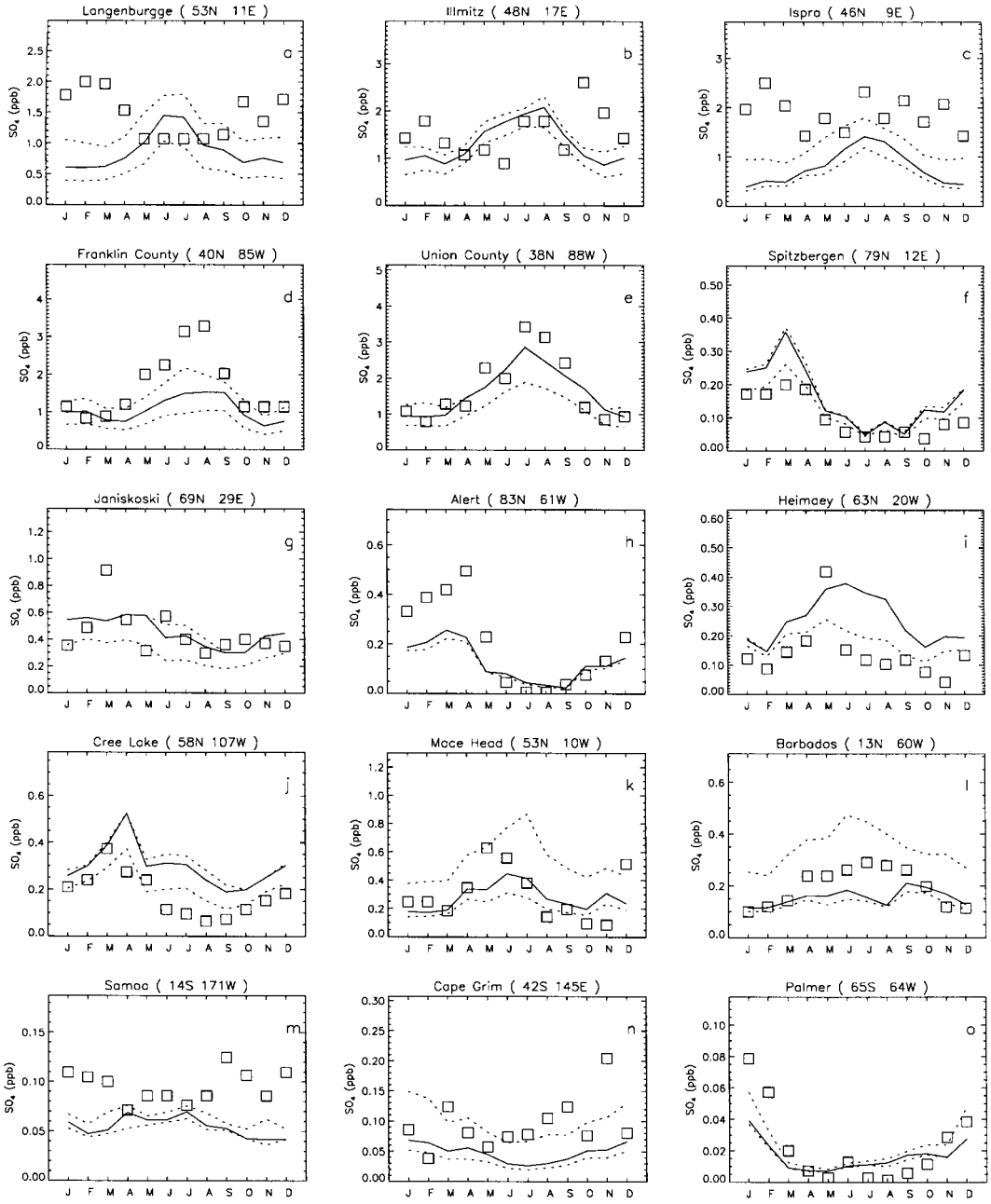

Fig. 1. Measured (squares, see text for references) and model calculated monthly averaged sulfate concentrations (ppb) at the surface. The dotted lines indicate maximum and minimum concentrations at the grid cell boundaries.

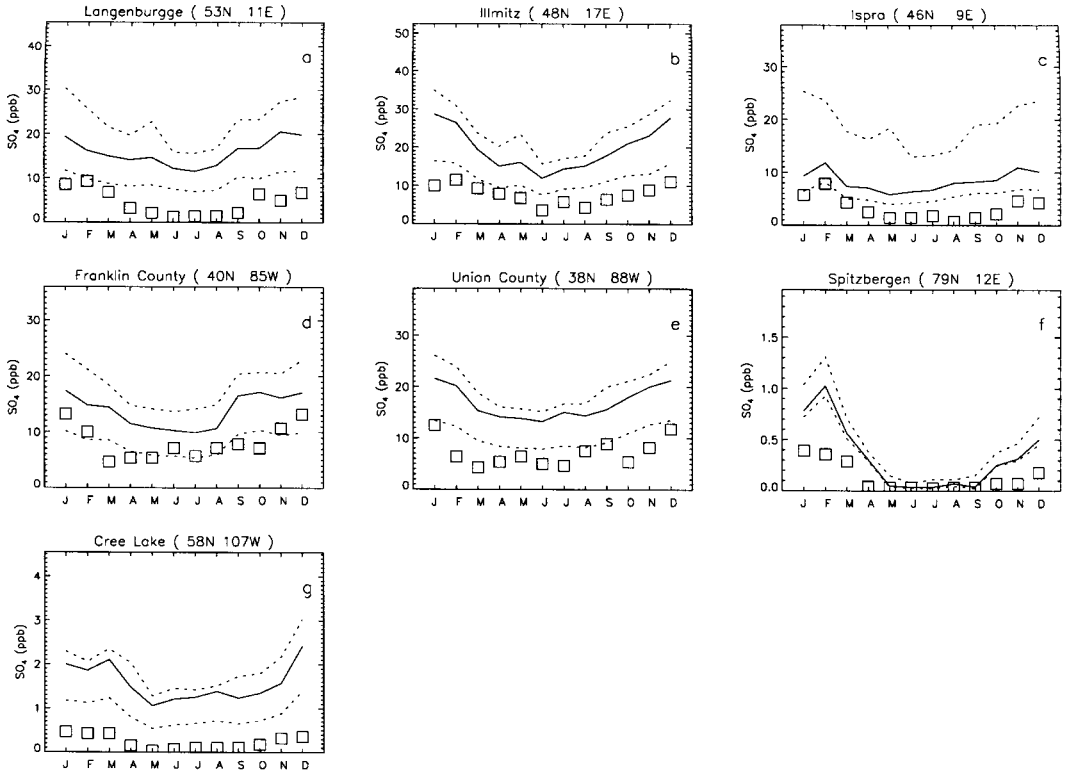

Fig. 2. As Fig. 1 but for SO_2.

3.2. *Calculated budgets and distributions*

Table 1 shows the calculated, yearly integrated, source and sink terms for SO_2 and sulfate and their tropospheric burden and lifetimes. Results are given for the present-day and the pre-industrial simulation. In the present-day simulation, 18% of the SO_2 is directly deposited, almost exclusively by dry deposition. This is lower than previous studies which use fixed dry deposition velocities, as discussed in Ganzeveld et al. (1998). The SO_2 dry deposition budget will be further affected by the vertical resolution in the lower troposphere, which is relatively fine in our model, and the fact that a substantial fraction of the anthropogenic SO_2 emissions is released in the layer above the surface layer. The calculated wet deposition of SO_2 is negligible. In previous studies, SO_2 wet deposition efficiencies between 4 and 20% were calculated (Chin et al., 1996; Table 9). We note that SO_2 that is scavenged by precipitating clouds or precipitation is not deposited as such but is

Table 1. *Simulated contemporary global budgets for SO_2 and sulfate*

	(Tg S yr^{-1})	(%)
total source	90	100
dry deposition SO_2	16	18
wet deposition SO_2	<1	0
oxidation	74	82
by OH		*18*
by O_3		*16*
by H_2O_2		*48*
SO_2 burden (Tg S)	0.61	
SO_2 lifetime (days)	2.4	
total source SO_4^{2-}	78	100
dry deposition SO_4^{2-}	17	22
wet deposition SO_4^{2-}	61	78
SO_4^{2-} burden (Tg S)	0.96	
SO_4^{2-} lifetime (days)	4.7	

mainly transformed to sulfate in the aqueous phase. In our model this fraction is 25 Tg S yr^{-1}, i.e., about 30%, and it does not contribute to the SO_2 but to the sulfate wet deposition flux.

Gas phase oxidation of SO_2 by OH contributes about 18% of the total SO_2 removal. The aqueous phase oxidation pathways by O_3 and H_2O_2 contribute 16 and 48%, respectively. The relative contribution of H_2O_2 to the total SO_2 oxidation (about 60%) has not changed significantly compared to Feichter et al. (1996). However, the contribution of O_3 has increased from about 10 to 20%, and that of OH has decreased, from about 30 to 22%. This is partly explained by the simultaneous calculation of both aqueous phase SO_2 oxidation pathways in our model. Oxidation by O_3 may be relatively efficient just after the cloud has formed but is not yet strongly acidified. This occurs mainly in clean to mildly polluted environments where concentrations of sulfate and HNO_3, which determine the initial cloud water pH, are relatively low. Further, the coupling between the sulfur cycle and tropospheric background chemistry enhances the contribution of oxidation by O_3 to the total SO_2 oxidation, as will be discussed in Section 4. Differences between the calculated climates of both models (versions 3 and 4) play an additional role (Feichter et al., 1997). We calculate a longer lifetime and a larger tropospheric burden of SO_2 compared to previous estimates, which range from 0.6 to 1.5 days and 0.2 to 0.43 Tg S, respectively (Chin et al., 1996; Table 9). This is largely associated with the coupling between the sulfur cycle and the tropospheric chemistry calculations as will be discussed in Section 4.

The total simulated source of sulfate (78 Tg S yr^{-1}) consists of sulfate production by SO_2 oxidation and a small contribution by direct sulfate emissions (3.3 Tg S yr^{-1}). Note that the sulfate source is 53 Tg S yr^{-1} when the SO_2 wet deposition term (see above) is not included, which is in good agreement with previous studies (between 49 and 62 Tg S yr^{-1}). We calculate that 22% of the sulfate is removed by dry deposition and 78% by wet deposition. Our explicit dry deposition scheme calculates higher sulfate deposition velocities than the constant deposition velocities used in the studies of Langner and Rodhe (1991) and Feichter et al. (1996) (Ganzeveld et al., 1988). Chin et al. (1996), who model dry deposition using a resistance-in-series scheme, calculate a sulfate dry deposition of 11%. The difference is probably associated with a more efficient nucleation scavenging of sulfate in convective clouds used by Chin et al. (1996), which enhances the sulfate wet deposition flux compared to our model. The calculated sulfate lifetime, 4.7 days, is in the range of previous estimates of 3.9–5.3 days, but our model calculates a larger sulfate burden of 0.96 Tg S compared to previous estimates of 0.55–0.77 Tg S.

Calculated sulfate concentrations in the NH free troposphere are considerably different for different global sulfur chemistry models. Simulated concentrations range between 25–50 ppt (Chin et al., 1996), 50–100 ppt (Feichter et al., 1996), 100–250 ppt (Langner and Rodhe, 1991), and about 250 ppt (Pham et al., 1995), whereas we calculate values up to 300 ppt. Comparison with the few observations in the free troposphere presented by Chin et al. (1996; Fig. 12) shows that the model may overestimate free tropospheric sulfate concentrations up to factor of 3 during summer over the NH remote oceans. This again indicates that the nucleation scavenging applied in our model is inefficient. We note that present-day global models apply parametrization for nucleation scavenging, for cloud and rain characteristics and for below cloud scavenging of sulfate by liquid ad solid precipitation that are highly simplified because of computational efficiency and will not yield representative results under all circumstances.

Fig. 3 displays the simulated yearly averaged sulfate columns (mg S m^{-3}). Maximum sulfate levels are calculated over North America, eastern Europe and central Asia, and eastern Asia. Because sulfate has a lifetime of about 5 days, it undergoes significant transport from the polluted areas to the oceans. Lower sulfate burdens are calculated over the Indian Ocean and the western tropical Pacific Ocean where rainout and washout of SO_2 and sulfate are relatively efficient, associated with convection in the Interhemispheric Tropical Convergence Zone (ITCZ). The model simulates a distinct maximum over southern Africa, due to local anthropogenic emissions from coal combustion and copper smelters (Spiro et al., 1992). Although these emissions are about an order of magnitude smaller than in Europe or North America, tropical convection efficiently

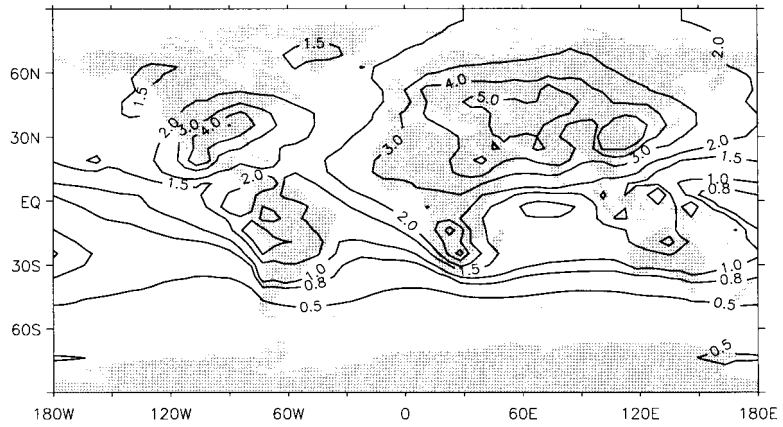

Fig. 3. Distribution of the annually averaged column sulfate burden (mg S m^{-2}).

transports SO_2 to the upper troposphere. Further, due to strong insolation in the tropics concentrations of OH and H_2O_2 are relatively high and SO_2 oxidation is relatively efficient. In the SH middle and high latitudes the model simulates sulfate columns below 0.5 mg S m^{-2}. Compared to the columns calculated by Chin and Jacob (1996), our model simulates columns that are about two times larger over the HN and roughly of the same magnitude over the SH. The discrepancy in the NH is mainly due to less efficient nucleation scavenging in our model. In the NH, sulfate columns are about 50% lower than results from Pham et al. (1995), who assume complete oxidation of SO_2 in a cloud.

We note that uncertainties associated with the DMS emission budget, transports and reaction pathways of DMS may affect the simulation of sulfate in remote maritime areas, especially in the SH. Calculated surface DMS concentrations are up to twice as high as observed, as was also found by Chin et al. (1996). They suggested that an unknown DMS oxidation pathway may play a role.

4. Coupled versus uncoupled sulfur-oxidant modeling

The approach to couple the sulfur cycle and the photochemistry schemes differs from previous studies that use monthly (and often zonally) averaged concentration distributions for H_2O_2, calculated without the sulfur cycle. To examine the effect of this coupling, the results of the coupled contemporary simulation are compared with two simulations performed with the sulfur cycle model in an off-line mode, i.e., decoupled from the photochemistry scheme. Instead, monthly average distributions for OH, H_2O_2, O_3, and NO_3 are used as input. For the first off-line simulation (A), the oxidant distributions are taken from a chemistry-GCM simulation without the sulfur cycle, whereas for the second off-line simulation (B) the oxidant distributions are taken from the coupled simulation. We focus on the NH middle and high latitudes (30°–90°N) where most anthropogenic emissions occur. Simulations A and B are carried out for a 1.5 year period, and the last 12 months are compared with the corresponding period from the coupled simulation. In this way, the three simulations consider the same meteorology.

Fig. 4 shows the seasonality of the SO_2 oxidation pathways and deposition for the three simulations between 30°–90°N. In the coupled simulation (Fig. 4a), the efficiency of the oxidation by H_2O_2 increases strongly between January and May, when H_2O_2 concentrations increase with photochemical activity. During summer, the gas phase OH oxidation contributes significantly to sulfate formation. The efficiency of H_2O_2 oxidation gradually decreases between May and August, and decreases more strongly between September and December as photochemical H_2O_2 production decreases. On the other hand, the oxidation by

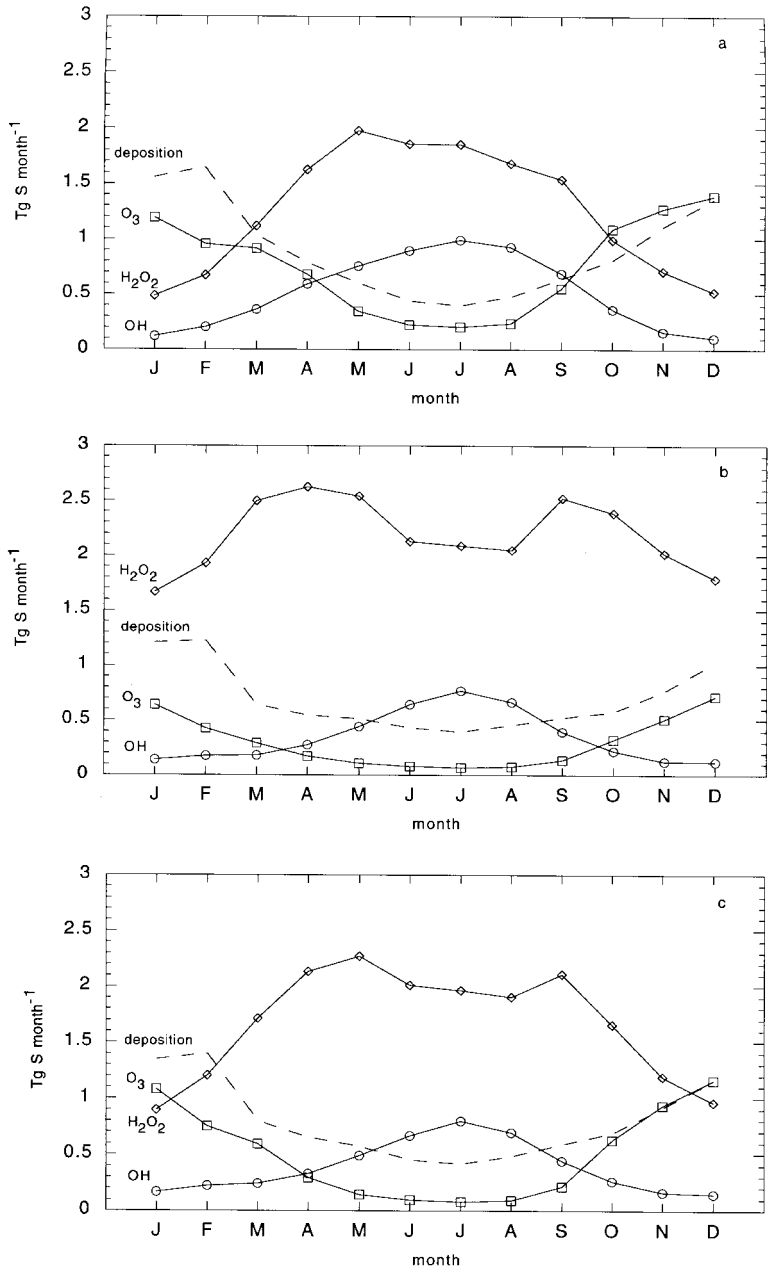

Fig. 4. Monthly integrated SO_2 oxidation and deposition rates (Tg S month^{-1}) for (a) the coupled simulation, (b) the off-line simulation A with oxidant fields from the chemistry-GCM without the sulfur cycle, and (c) the off-line simulation B with oxidant fields from the coupled simulation. Shown are the SO_2 oxidation by H_2O_2 (diamonds), by O_3 (squares), and by OH (circles) and the SO_2 deposition (dashed line).

O_3 and the dry deposition of SO_2 maximize during winter and minimize during summer.

During winter, spring and autumn, the H_2O_2 oxidation efficiency calculated in the off-line simulations exceeds that in the coupled simulation, with differences in January up to 200% for simulation A and 90% for simulation B (Fig. 4b, c). It should be emphasized that the monthly averaged H_2O_2 distributions in the coupled simulation and in off-line simulation B are identical. Since the oxidation by H_2O_2 is pH-independent over a wide range, the differences between the coupled and off-line B simulations are associated with temporal variabilities of H_2O_2 concentrations. Under polluted conditions, the photochemical production of H_2O_2 often becomes a limiting factor for SO_2 oxidation in the coupled simulation. For example, at night H_2O_2 may be depleted by reaction with dissolved SO_2, but it is not replenished until daybreak when photochemical activity commences, leading to an accumulation of SO_2. In simulation B, at the beginning of each time step H_2O_2 is reset to its monthly average value regardless the time of day. Thus, compared to the off-line simulation, the oxidant limitation is stronger when the H_2O_2 temporal variability is accounted for. In simulation A, the oxidation efficiency is further enhanced due to the higher H_2O_2 concentrations calculated in the absence of SO_2 oxidation. Note that differences between the coupled and the off-line simulations are relatively small in summer, indicating that oxidant limitation is not important then.

Table 2 presents the simulated yearly SO_2 budgets for 30°–90°N for the three simulations. The simulated SO_2 source in this area is 49 Tg S yr^{-1}, of which a small fraction, 2 Tg S yr^{-1}, originates from DMS. In the coupled simulation, 15 Tg SO_2 yr^{-1} (as S) is removed by H_2O_2. In simulations A and B this is 26 and 21 Tg S yr^{-1}, respectively. As a consequence of the more efficient oxidation of SO_2 by H_2O_2 in A and B, the oxidation by OH and O_3 and SO_2 dry deposition are less efficient than in the coupled simulation. The computed SO_2 burdens and lifetimes are significantly smaller, which is consistent with results from previous off-line model calculations. Note that the SO_2 emissions and sinks in Table 2 do not balance: the remainder, about 7 Tg S yr^{-1}, is transported southward of 30°N. Since SO_2 emissions are relatively small in the tropics and the SO_2 lifetime in the tropics is relatively short as a result of relatively high OH and H_2O_2 concentrations, it may be assumed that the northward SO_2 flux is relatively small. In the coupled simulation and in simulations A and B, the sulfate produced by SO_2 oxidation is 30, 34, and 32 Tg S yr^{-1}, respectively. The calculated regional sulfate burden is about the same in the three simulations, $\sim$0.32 Tg S, and the regional sulfate lifetime varies between 3.4 days for simulation A and 3.8 days for the coupled simulation.

Despite the almost equal sulfate burdens in the coupled simulation and off-line simulation A, significant differences are found between calculated column sulfate distributions. Due to the smaller oxidant limitation in the off-line simulation the SO_2 lifetime is shorter and sulfate formation takes place closer to where the SO_2 emissions occur. Hence, sulfate columns in the off-line simulation are larger near emission areas and generally smaller over remote ares. The results presented in Fig. 4 indicate that the coupled and the off-line simulations differ mostly during winter when the oxidant limitations is most effective. The winter sulfate burden calculated in the coupled simulation and the off-line simulation A is 0.19 and 0.24 Tg S, respectively, with the largest column differences occurring over the NH high latitude continents. Summer sulfate burdens are 0.47 Tg S in both simulations and differences between sulfate column distributions are relatively small. Because the effect of coupling the photo-oxidant chemistry and the sulfur cycle on the atmospheric sulfate loading in the polluted NH is relatively large in winter when insolation is low but small in summer when insolation is high, we conclude that the coupling will have a minor impact on the calculation of the direct and indirect radiative forcing by sulfate aerosol.

We remark that simulations A and B generally predict higher surface sulfate concentrations in the NH in winter than the coupled simulation. More specifically, the off-line models show a better agreement with observed surface concentrations for Ispra and Alert and a worse agreement for Spitzbergen, Heimaey and Cree Lake. Due to more efficient oxidation, surface SO_2 concentrations are also represented somewhat better in the off-line simulations. Nevertheless, in a coupled scheme the gas and aqueous phase SO_2 oxidation are represented more realistically than in an off-

Table 2. *Simulated SO_2 and sulfate budgets at 30°–90°N for the simulations with coupled and off-line sulfur-oxidant chemistry*

	Coupled		Off-line A		Off-line B	
	(Tg S yr^{-1})	(%)	(Tg S yr^{-1})	(%)	(Tg S yr^{-1})	(%)
total source	49	100	49	100	49	100
dry deposition SO_2	11	22	8	17	10	20
oxidation	30	62	34	70	32	66
by OH	*6*	*13*	*4*	*9*	*5*	*10*
by O_3	*9*	*19*	*4*	*7*	*6*	*12*
by H_2O_2	*15*	*31*	*26*	*54*	*21*	*44*
SO_2 burden (Tg S)	0.36		0.23		0.28	
SO_2 lifetime (days)	2.7		1.7		2.1	
SO_4^{2-} burden (Tg S)	0.32		0.32		0.33	
SO_4^{2-} lifetime (days)	3.8		3.4		3.7	

line scheme. These results support the earlier suggestion that additional reaction mechanisms play a role in the oxidation of SO_2 which are not yet accounted for in current 3D models.

5. Simulation of cloud optical properties

5.1. Method

In this section, we investigate how the sulfate distribution affects cloud optical properties. At each time step we combine the simulated sulfate concentrations and the ECHAM cloud distributions to calculate effective cloud drop radii. We use a relation between sulfate and CDNC derived from measurements from the Ground Based Cloud Experiment (GCE) in April–May of spring 1993 at Great Dun Fell (T. Choularton, personal communication):

$$\mathrm{CDNC} = 530\{1 - \exp(-0.61 m_{\mathrm{SO_4}})\} \quad (4a)$$

with CDNC in cm^{-3} and m_{SO_4} in μg sulfate m^{-3}. Fig. 5 shows the measured sulfate concentrations before cloud formation versus CDNC, and the calculated fit through the data. Information about the measurements can be found in Choularton et al. (1997). The air masses that were sampled during GCE varied from relatively unpolluted marine air to relatively polluted continental air. Measured sulfate concentrations ranged between 0.5 and 9 μg m^{-3}. This roughly coincides with the simulated boundary layer sulfate concentrations in the NH, on average 2–5 μg m^{-3} over continents and 0.5–1 μg m^{-3} over the ocean. Fig. 6 shows the Great Dun Fell (GDF) relation and the relations previously used by Boucher and Lohmann (1995):

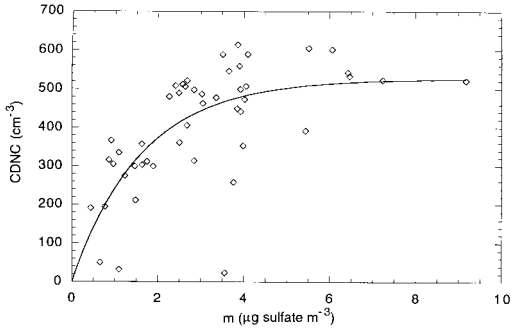

Fig. 5. Sulfate concentration (μg sulfate m^{-3}) beneath the cloud base plotted against cloud droplet concentration (cm^{-3}) (Choularton et al., 1997). The solid line indicates the fit through the data points (eq. (4a)).

$$\begin{aligned} \mathrm{CDNC_{cont}} &= 10^{2.24 + 0.257 \log m_{\mathrm{SO_4}}}, \\ \mathrm{CDNC_{ocean}} &= 10^{2.06 + 0.48 \log m_{\mathrm{SO_4}}}, \end{aligned} \quad (4b)$$

giving the relation between sulfate mass and cloud droplet number concentration in stratiform continental and maritime clouds, respectively, and by Jones et al. (1994):

$$\mathrm{CDNC} = 375\{1 - \exp(-0.42 m_{\mathrm{SO_4}})\} \quad (4c)$$

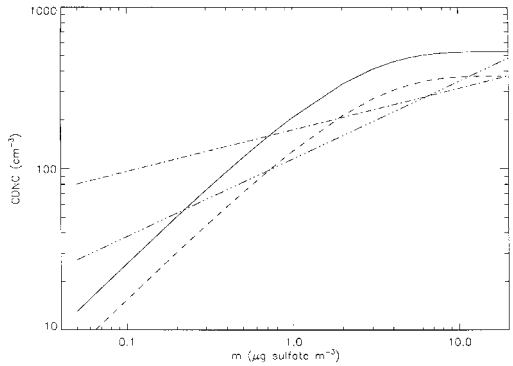

Fig. 6. Relations between the sulfate mass concentration and the cloud droplet concentration from the Great Dun Fell cloud experiment (eq. (4a), solid line), from Jones et al. (1994) (Eq. (4c), dashed line), and from Boucher and Lohmann (1995) (eq. (4b)) for maritime (dashed-dotted line) and continental clouds (dashed-dotted-dotted line).

We note that the Jones et al. relation originally depends on aerosol particle number concentration; eq. (4c) is derived from Jones and Slingo (1996, Fig. 3). CDNC calculated with the GDF and the Jones et al. relations increase with sulfate concentration in a similar fashion, but the GDF relation predicts 40–100% more cloud droplets depending on sulfate mass. Eqs. (4a) and (4c) are applied to both maritime and continental clouds. The Boucher and Lohmann relation displays a weaker increase of CDNC with sulfate for sulfate concentrations below approximately 3 μg m^{-3} (about 800 pptv at the surface). Further, it predicts a larger CDNC when the sulfate concentration is below approximately 0.5 μg m^{-3} over land (about 130 pptv) and 0.2 μg m^{-3} over sea (about 50 pptv). In the GDF and the Jones et al. (1994) relations, CDNC approaches zero much faster with decreasing sulfate mass. This indicates that the Boucher and Lohmann relation to a certain degree accounts for particles other than sulfate which may contribute significantly to CDNC under low sulfate conditions. Important in this respect are remote oceans, where seasalt particle formation occurs at the surface through the bursting of air bubbles resulting from entrainment of air induced by wind stress (O'Dowd et al., 1997). O'Dowd and Smith (1993) found that under clean marine conditions and moderate to high wind speeds, seasalt aerosol can readily dominate the accumulation mode aerosol. Since the accumulation mode particle concentration generally dominates the amount of cloud condensation nuclei (CCN) it can be expected that the GDF and Jones et al. relations underestimate CDNC for clean maritime conditions at higher wind speeds. To improve the calculation of cloud droplet effective radii under such conditions we have derived an expression for CDNC as function of sulfate mass and wind speed. A 1D rising parcel model (Roelofs, 1992) with initial updraft velocity of 20 cm s^{-1} is applied to cloud formation simulations using detailed three-modal seasalt aerosol size distributions that depend on wind speed (O'Dowd and Smith, 1993) as input. The input aerosol further consisted of a nss-sulfate accumulation mode, of which the mass is varied by adjusting the number concentration. From simulations with different wind speeds and nss-sulfate masses the following fit was obtained:

$$\mathrm{CDNC} = 136.5 m_{\mathrm{SO_4}} + \exp(0.22 U_{10}), \qquad (5)$$

where U_{10} is the 10 m wind speed. According to this relation and for a wind speed of 10 m s^{-1}, 40% of the CDNC form on seasalt particles when the sulfate mass is 0.1 μg m^{-3}, and 15% when the sulfate mass is 0.4 μg m^{-3}. Compared to the GDF sulfate-CDNC relation, the seasalt-CDNC relation (5) predicts higher CDNC when the wind speed exceeds 10 m s^{-1} and sulfate concentrations are below approximately 0.2 μg m^{-3}. In the global model we apply the seasalt-CDNC relationship between the ocean surface and an altitude of 2 km. Whenever sulfate concentrations are below 0.4 μg m^{-3}, CDNC from equations (4a) and (5) are compared and the highest CDNC is chosen.

The effective cloud drop radius r_{eff} is calculated by:

$$r_{\mathrm{eff}} = \left(\frac{3\mathrm{LWC}}{4\pi \rho_{\mathrm{w}} \kappa \, \mathrm{CDNC}} \right)^{1/3}, \qquad (6)$$

where LWC is the liquid water content calculated by the climate model, ρ_{w} is the specific mass of liquid water, and κ is the cube ratio between the mean volume radius and the effective radius of the cloud drop spectrum. Martin et al. (1994) derived values for κ for continental and maritime clouds of 0.67 and 0.80, respectively. In our calculations we use an average value of 0.75, following the approach by Boucher and Lohmann (1995).

5.2. Results

Fig. 7 shows zonally averaged effective drop radii for continental and maritime clouds, simulated by the chemistry-GCM. Also shown are zonally averaged effective droplet radii that are retrieved from data from the International Satellite Cloud Climatology Project (ISCCP) (Han et al., 1994). For maritime clouds in the subtropics, the simulated effective cloud drop radii are between 11 and 12 μm. This is about 1 μm smaller than observed, but within the 2 μm uncertainty of the retrieved values (Han et al., 1994). The latitudinal variability of maritime cloud drop sizes in the SH agrees well with the observations, with a maximum of 13 μm at 20°S (observed: 14 μm). Tropospheric sulfate concentrations are relatively low in SH middle and high latitudes, between 0.1 and 0.3 μg m^{-3}, so that seasalt aerosol effectively co-determines the CDNC. The simulated effective cloud drop radii in this region are around 12 μm, but radii of 2 to 6 μm larger are calculated without the above seasalt-CDNC relationship. Observed maritime effective cloud drop radii in the NH do not vary significantly with latitude, but the model simulates a decrease from 11 μm in the tropics of 9 μm at 50°N. We note that a decrease is also calculated by Boucher and Lohmann (1995; results from ECHAM) and by Chuang et al. (1997).

Simulated effective radii over the continents are about 2 μm smaller than observed at lower latitudes. At higher latitudes the model underestimates the radii by about 3 μm in the NH. Boucher and Lohmann (1995), who used ECHAM3 in their study, obtained even lower values and attributed this to the fact that simulated liquid water contents in continental clouds are relatively low compared to maritime clouds. A considerable improvement in this respect may be expected when a finer resolution of the model is used. Chen and

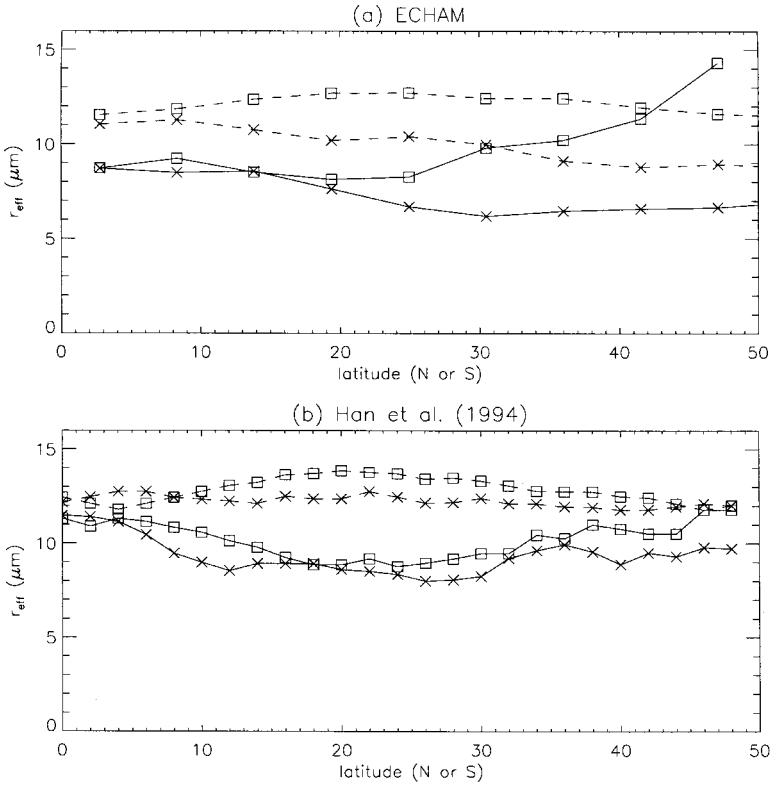

Fig. 7. Simulated annual and zonal average effective droplet radii (μm). Solid lines represent continental clouds and dotted lines represent maritime clouds in the NH (crosses) and SH (squares).

Roeckner (1997) found that the climatological mean and space-time variations of total cloud amount and cloud liquid water path simulated in ECHAM in the T42 resolution (2.8° horizontally) are in reasonable agreement with observations from ISCCP, although some discrepancies remain. South of 25°S, the simulated and the observed drop radii over land increase with latitude, but the simulated radii are larger by about 3 μm. Between 30°–50°S, the calculation of effective cloud drop radii over continents is determined by the southern part of South America where sulfur emissions are relatively low. Apparently, other components than sulfate play a significant role in cloud nucleation in this region. Effective radii calculated by Chuang et al. (1997), who did not use a sulfate-CDNC relation but calculated the effective cloud drop radii using a mixture of pre-existing aerosols and anthropogenic sulfate, are in better agreement with the observed radii.

We have also applied the parameterizations of Boucher and Lohmann (1995) eq. (4b) and of Jones et al. (1994) (eq. (4c) extended with the seasalt-CDNC relation) in the model. Table 3 presents a comparison between observed and calculated effective radii for different surface types and geographical region. The data of Han et al. (1994) indicate that the effective cloud drop radii over land are on average 3.3 μm smaller than over the ocean, and that radii in the NH are smaller by about 0.7 μm than in the SH. With the GDF relation we calculate a land-sea difference of 3.9 μm, which agrees well with the observations in view of the uncertainty, but a hemispheric difference of 2.6 μm mainly due to the underestimation of simulated effective radii in the NH. We note that the overestimation of sulfate concentrations in the NH free troposphere, discussed in Section 3, probably does not influence the calculation of the drop radii which is restricted to lower tropospheric clouds. For the different regions the discrepancies between modelled and observed values are generally below 1.5 μm, especially in the SH. We conclude that the GDF sulfate-CDNC relationship (eq. (4a)) combined with the seasalt-CDNC relation, (eq. (5)), yields realistic effective cloud drop radii for the sulfate and cloud distributions calculated by ECHAM.

The Boucher and Lohmann relation, applied to our model, yields a good agreement between modelled and observed effective radii, especially over the ocean. Over land the simulated radii are smaller than observed by about 1.3 μm. The Jones et al. relation is qualitatively similar to the GDF relation but predicts a lower CDNC, which translates to larger effective radii by 1.3 to 2 μm. In our model the Jones et al. relation yields good results in the NH but considerably overestimates effective radii in the SH. Note that Jones and Slingo (1996) find a good agreement between modelled and observed values over the ocean but an overestimation over land. In their study they used the sulfate distribution of Penner et al. (1994) and cloud characteristics from the Hadley Centre

Table 3. *Effective cloud drop radii (μm) by the three different sulfate-CNDC relations compared with the satellite retrievals of Han et al. (1994)*

	Han et al.	GDF	Boucher and Lohmann (1995)	Jones et al. (1994)
Global (45°S–45°N)	11.4	10.4	10.7	11.9
NH	11.0	9.1	9.7	10.8
SH	11.7	11.7	11.7	13.1
Land	8.5	7.5	7.1	9.3
NH land	8.2	6.9	6.8	8.5
SH land	9.0	8.8	7.7	11.1
Ocean	11.8	11.4	12.0	12.8
NH ocean	11.6	10.3	11.3	12.0
SH ocean	12.0	12.2	12.5	13.5

climate model. This demonstrates that differences between calculated sulfate fields, cloud distributions and cloud liquid water content (and thus differences between GCMs) potentially have a significant impact on derived effective radii and hence on the calculated indirect forcing as noted earlier by Boucher and Lohmann (1995). This is also illustrated by two simulations of effective cloud drop radii using relation D of Boucher and Lohmann (1995). The effective cloud drop radii calculated by Boucher and Lohmann (1995; Table 4) and by Jones and Slingo (1996; Table 1) differ by 1 to 4 μm. Using relation A of Boucher and Lohmann, we calculate effective radii that are up to 2.5 μm larger than their original model results (Boucher and Lohmann, 1995; Table 4). The results indicate that, on average, the sensitivity of effective cloud drop radius calculations to uncertainties in the sulfate and cloud fields is of the order of a few micrometers.

For NH middle and high latitudes in a pre-industrial atmosphere, sulfate concentrations below 50 pptv ($0.2\ \mu g\ m^{-3}$) are estimated (Boucher and Lohmann, 1995). Under these conditions other chemical aerosol species, e.g., organic material, will play a significant role in the determination of CDNC. The Jones et al. and the GDF relations display a stronger dependence of CDNC of sulfate in the range 0.2–0.5 $\mu g\ m^{-3}$ than the Boucher and Lohmann relation or the approach of Chuang et al. (1997), and they probably underestimate the importance of other aerosol species. Therefore, applying the GDF relation to the calculation of cloud optical properties in a pre-industrial atmosphere will probably lead to an underestimation of CDNC and, hence, an overestimation of the inferred magnitude of the indirect aerosol climate forcing.

6. Conclusions

We presented a numerical model in which the calculations for meteorology, gas phase photochemistry, and aqueous phase sulfur chemistry and removal mechanisms of trace species have been coupled. Until now, global 3D models have neglected or underestimated the oxidant (i.e., H_2O_2) limitation of SO_2 oxidation in the aqueous phase, particularly during winter when photochemical activity is low. The effect of oxidant limitation is more pronounced in our coupled model than in models that use monthly averaged oxidant distributions as input. Firstly, H_2O_2 distributions are generally calculated without considering the sulfur cycle, so H_2O_2 concentrations used in the off-line models are higher. Secondly, the use of monthly averaged H_2O_2 distributions neglects the temporal variability of H_2O_2, for example, associated with the slow replenishment of H_2O_2 after its depletion by SO_2 in winter. By neglecting this variability the oxidant limitation is underestimated. Since in the polluted NH the oxidant limitation is most effective during winter and relatively small in summer, the coupling between the sulfur cycle and the photochemistry is expected to have a minor impact on the calculation of the indirect and direct radiative forcing by sulfate.

As a consequence of the enhanced oxidant limitation, the coupled model calculates smaller H_2O_2 and larger O_3 contributions to the total SO_2 oxidation than off-line sulfur models. We note that uncertainties in cloud pH may have a significant effect on the simulated sulfate formation through oxidation by O_3. Our model calculates somewhat lower SO_2 dry deposition velocities compared to the fixed SO_2 dry deposition values used in earlier studies. Consequently, the global tropospheric SO_2 content is larger. The model also simulates a rather large atmospheric sulfate content probably associated with a relatively low wet scavenging efficiency in convective clouds.

The model systematically overestimates surface SO_2 concentrations in polluted regions in Europe and North America. On the other hand, surface sulfate concentrations are somewhat underestimated in these areas. It should be emphasized that the coupling between the comprehensive gas phase chemistry scheme and the sulfur cycle even enhances the discrepancies between simulated and observed sulfate concentrations, especially in winter, due to the stronger oxidant limitation. However, it supports the suggestion that additional reaction mechanisms play a role in the oxidation of SO_2 than the ones accounted for in current 3D models.

From measurements in the Great Dun Fell cloud experiment in 1993 an empirical formulation has been derived that relates measured sulfate aerosol concentrations to cloud droplet number concentrations. We have added a relationship

between aerosol generation and wind speed to account for the effect of seasalt aerosols in remote marine locations. Each time step we calculated effective cloud drop radii using simulated sulfate and cloud liquid water distributions and the 10 m wind speed. Comparison of calculated zonlly averaged effective cloud drop radii with satellite retrieved values indicates that the sulfate-CDNC relation measured at Great Dun Fell appears representative for a large part of the contemporary atmosphere, although a small discrepancy exists for the NH which may be attributed to uncertainties in the satellite retrieval as well as the simulated sulfur distributions and cloud characteristics. Calculations based on previously used relations indicate a sensitivity to the sulfate and cloud distributions that is of the order of a few micrometers. We emphasize that the uncertainties connected with the representation of some of the governing cloud processes in present-day global models may be quite large. The models necessarily contain parametrizations for cloud cover, liquid water content, precipitation formation and for in-cloud and below-cloud scavenging of sulfate that highly simplify or neglect the dependence on the size distributions of aerosols and cloud and rain drops. The results of this study emphasize the need for more detailed cloud microphysical parametrizations in global chemistry-climate models.

7. Acknowledgement

This work has been performed within EC project no. EV5V-CT94-0450, the EC project SINDICATE (DG XII), and the NOP-II project 951258 (Netherlands organization for scientific research). We thank Mijke Doorenbosch for her contribution with the 1D parcel model. Further, we thank the Max-Planck-Institute for Meteorology and the Deutche Klimarechenzentrum in Hamburg for the use of computer facilities and support.

REFERENCES

Albrecht, B. A. 1989. Aerosols, Cloud microphysics, and fractional cloudiness. *Science* **245**, 1227–1230.

Atkinson, R., Baulch, D. L., Cox, R. A., Hampson, R. F. Jr., Kerr, J. A. and Troe, J. 1992. Evaluated kinetic and photochemical data for atmospheric chemistry: Supplement IV. *Atmos. Environ.* **26A**, 1187–1230.

Ayers, G. P., Ivey, J. P. and Goodman, H. S. 1986. Sulfate and methanesulfonate in the maritime aerosol at Cape Grim, Tasmania. *J. Atmos. Chem.* **4**, 173–185.

Ayers, G. P., Ivey, J. P. and Gillett, R. W. 1991. Coherence between seasonal cycles of dimethyl sulphide, methanesulphonate and sulpate in marine air. *Nature* **349**, 404–406.

Barrie, L. A. and Bottenheim, J. W. 1991. Sulphur and nitrogen pollution in the Arctic atmosphere. In: *Pollution of the Arctic atmosphere* (ed. W. Sturges), 334 pp. Elsevier, New York.

Bates, T. S., Lamb, B. K., Guenther, A., Dignon, J. and Stoiber, R. E. 1992. Sulfur emissions to the atmosphere from natural sources. *J. Atmos. Chem.* **14**, 315–337.

Benkovitz, C. M., Scholtz, M. T., Pacyna, J., Tarrasón, L., Dignon, J., Voldner, E. C., Spiro, P. A., Logan, J. A. and Graedel, T. E. 1996. Global gridded inventories of anthropogenic emissions of sulfur and nitrogen. *J. Geophys. Res.* **101**, 29239–29253.

Boucher, O. and Lohmann, U. 1995. The sulfate-CCN-cloud albedo effect. A sensitivity study with two general circulation models. *Tellus* **47B**, 281–300.

Charlson, R. J., Langner, J., Rodhe, H., Leovy, C. B. and Warren, S. G. 1991. Perturbation of northern hemisphere radiative balance by backscattering from anthropogenic sulfate aerosols. *Tellus* **43A/B**, 152–163.

Charlson, R. J., Schwartz, S. E., Hales, J. M., Cess, R. D., Coakley, J. A., Hansen, J. E. and Hofmann, D. J. 1992. Climate forcing by anthropogenic aerosols. *Science* **255**, 423–430.

Chen, C.-T. and Roeckner, E. 1996. Validation of the Earth radiation budget as simulated by the Max Planck Institute of Meteorology general circulation model ECHAM4 using satellite observations of the Earth Radiation Budget Experiment. *J. Geophys. Res.* **101**, 4269–4278.

Chen, C.-T. and Roeckner, E. 1997. Cloud simulations with the Max Planck Institute for Meteorology general circulation model ECHAM4 and comparison with observations. *J. Geophys. Res.* **102**, 9335–9350.

Chin, M., Jacob, D. J., Gardner, G. M., Foreman-Fowler, M., Spiro, P. A. and Savoie, D. L. 1996. A global three-dimensional model of tropospheric sulfate. *J. Geophys. Res.* **101**, 18667–18690.

Chin, M. and Jacob, D. J. 1996. Anthropogenic and natural distributions to tropospheric sulfate: a global model analysis. *J. Geophys. Res.* **101**, 18691–18699.

Choularton, T. W. et al. 1997. The Great Dun Fell cloud experiment 1993: an overview. *Atmos. Environ.* **31**, 2393–2405.

Chuang, C. C., Penner, J. E., Taylor, K. E., Grossman, A. S. and Walton, J. J. 1997. An assessment of the radiative effects of anthropogenic sulfate. *J. Geophys. Res.* **102**, 3761–3778.

Crutzen, P. J. and Zimmermann, P. H. 1991. The changing photochemistry of the troposphere. *Tellus* **43A/B**, 136–151.

Dentener, F. J., Carmichael, G. R., Zhang, Y., Lelieveld, J. and Crutzen, P. J. 1996. The role of mineral aerosol as a reactive surface in the global troposphere. *J. Geophys. Res.* **101**, 22869–22889.

EMEP Data Report 1986–1992, 1988–1994. Part 2: monthly and seasonal summaries. *EMEP/CCC-Reports 7/88, 2/89, 5/90, 3/91, 3/92, 5/93, 5/94*. Norwegian Institute For Air Research, Lillestrøm, Norway.

Feichter, J., Kjellström, E., Rodhe, H., Dentener, F., Lelieveld, J. and Roelofs, G. J. 1996. Simulation of the tropospheric sulfur cycle in a global climate model. *Atmos. Environ.* **30**, 1693–1707.

Feichter, J., Lohmann, U. and Schult, I. 1997. The atmospheric sulfur cycle in ECHAM-4 and its impact on the shortwave radiation. *Clim. Dyn.* **13**, 235–246.

Galloway, J. N., Savoie, D. L., Keene, W. C. and Prospero, J. M. 1993. The temporal and spatial variability of scavenging ratios for nss-sulfate, nitrate, methanesulfonate and sodium in the atmosphere over the North Atlantic Ocean. *Atmos. Environ.* **27A**, 235–250.

Ganzeveld, L. N. and Lelieveld, J. 1995. Dry deposition parameterization in a chemistry — general circulation model and its influence on the distribution of chemically reactive trace gases. *J. Geophys. Res.* **100**, 20999–21012.

Ganzeveld, L. N., Lelieveld, J. and Roelofs, G. J. 1998. A dry deposition parametrization for sulfur oxides in a chemistry-general circulation model. *J. Geophys. Res.*, in press.

Ghan, S. J., Leung, L. R., Easter, R. C. and Abdul-Razzak, H. 1997. Prediction of cloud droplet number in a general circulation model. *J. Geophys. Res.* **102**, 21777–21794.

Hao, W. M. and Liu, M. H. 1994. Spatial and temporal distribution of tropical biomass burning. *Global Biogeochem. Cycles* **8**, 495–503.

Han, Q., Rossow, W. B. and Lacis, A. A. 1994. Near-global survey of effective droplet radii in liquid water clouds using ISCCP data. *J. Climate* **7**, 465–497.

Haskins, R. D., Barnett, T. P., Tyree, M. M. and Roeckner, E. 1995. Comparison of cloud fields from atmospheric general circulation model, *in situ* and satellite measurements. *J. Geophys. Res.* **100**, 1367–1378.

Hicks, B. B., Baldocchi, D. D., Meyers, T. P., Hosker, R. P. Jr. and Matt, D. R. 1987. A preliminary multiple resistance routine for deriving dry deposition velocities from measured quantities. *Water, Air, Soil Pollut.* **36**, 311–330.

Intergovernmental Panel on Climate Change IPCC 1996. *Climate change 1995*, edited by J. T. Houghton, L. G. Meira Filho, B. A. Callander, N. Harris, A. Kattenberg, and K. Maskell. Cambridge University Press, Cambridge, pp. 65–130.

Jacob, D. J. et al. 1997. Evaluation and intercomparison of global atmospheric transport models using ^{222}Rn and other short-lived tracers. *J. Geophys. Res.* **102**, 5953–5970.

Jones, A., Roberts, D. L. and Slingo, A. 1994. A climate model study of the indirect radiative forcing by anthropogenic sulfate aerosols. *Nature* **370**, 450–453.

Jones, A. and Slingo, A. 1996. Predicting cloud-droplet effective radius and indirect sulphate aerosol forcing using a general circulation model. *Q. J. R Meteorol. Soc.* **122**, 1573–1595.

Kasibhatla, P., Chameides, W. L. and John, J. St. 1997. A three-dimensional global model investigation of seasonal variations in the atmospheric burden of anthropogenic sulfate aerosols. *J. Geophys. Res.* **102**, 3737–3760.

Kiehl, J. T. and Briegleb, B. P. 1993. The relative roles of sulfate aerosols and greenhouse gases in climate forcing. *Science* **260**, 311–314.

Langner, J. and Rodhe, H. 1991. A global three-dimensional model of the global sulfur cycle. *J. Atmos. Chem.* **13**, 225–236.

Lelieveld, J., Roelofs, G. J., Ganzeveld, L., Feichter, J. and Rodhe, H. 1997. Terrestrial sources and distribution of atmospheric sulphur. *Phil. Trans. Roy. Soc.* **352**, 149–158.

Li, S.-M. and Barrie, L. A. 1993. Biogenic sulfur aerosol in the Arctic troposphere: 1. Contributions to total sulfate. *J. Geophys. Res.* **98**, 20613–20622.

Lohmann, U. and Feichter, J. 1997. Impact of sulfate aerosols in albedo and lifetime of clouds: a sensitivity study with the ECHAM4 GCM. *J. Geophys. Res.* **102**, 13685–13700.

Martin, G. M., Johnson D. W. and Spice, A. 1994. The measurement and parameterisation of effective radius of droplets in warm stratocumulus clouds. *J. Atmos. Sci.* **51**, 1823–1842.

Mason, B. J. 1971. *The physics of clouds*, Clarendon Press, Oxford, pp. 593–613.

O'Dowd, C. D. and Smith, M. H. 1993. Physico-chemical properties of aerosol over the northeast Atlantic: evidence for wind speed related sub-micron sea-salt aerosol production. *J. Geophys. Res.* **98**, 1132–1136.

O'Dowd, C. D. Smith, M. H., Consterdine, I. E. and Lowe, J. A. 1997. Marine aerosol, seasalt, and the marine sulphur cycle: a short review. *Atmos. Environ.* **31**, 73–80.

Penner, J. E., Atherton, C. S. and Graedel, T. E. 1994. Global emissions and models of photochemically active compounds. In: *Global atmospheric biospheric chemistry*, edited by R. G. Prinn. Plenum, New York, pp. 223–247.

Pham, M., Müller, J.-F., Brasseur G. P., Granier, C. and Mégie, G. 1995. A three-dimensional study of the tropospheric sulfur cycle. *J. Geophys. Res.* **100**, 26061–26092.

Prospero, J., Savoie, D. L., Arimoto, R., Olafsson, H. and Hjartarson, H. 1995. Sources of aerosol nitrate and non-sea-salt sulfate in the Iceland region. *Sci. Total Environ.* **160/161**, 181–191.

Pruppacher, H. R. and Klett, J. D. 1978. *Microphysics of clouds and precipitation*, D. Reidel, 714 pp.

Rasch, P. J. and Williamson, D. 1990. Computational aspects of moisture transport in global models of the atmosphere. *Q. J. R. Meteorol. Soc.* **116**, 1071–1090.

Roeckner, E., Rieland, M. and Keup, E. 1991. Modelling of clouds and radiation in the ECHAM model. In: ECMWF/WCRP Workshop on clouds, radiative transfer and the hydrological cycle. ECMWF, 199–222.

Roeckner, E., Siebert, T. and Feichter, J. 1995. Climatic response to anthropogenic sulfate forcing simulated with a general circulation model. In: *Aersol forcing of climate* (ed. R. J. Charlson and J. Heintzenberg). John Wiley and Sons, New York, 349–362.

Roeckner, E., Arpe, K., Bengtsson, L., Christoph, M., Claussen, M., Dümenil, L., Esch, M., Giorgetta, M., Schlese, U. and Schulzweida, U. 1996. *Simulation of the present-day climate with the ECHAM model: Impact of model physics and resolution.* Report no. 218. Max-Planck-Institute for Meterology, Hamberg, Germany.

Roelofs, G. J. 1992. On the drop and aerosol size dependendence of aqueous phase sulfate formation in a continental cumulus cloud. *Atmos. Environ.* **26A**, 2309–2321.

Roelofs, G. J. 1993. A cloud chemistry sensitivity study and comparison of explicit and bulk cloud model performance. *Atmos. Environ.* **27A**, 2255–2264.

Roelofs, G. J. and Lelieveld, J. 1995. Distribution and budget of O_3 in the troposphere calculated with a chemistry — general circulation model. *J. Geophys. Res.* **100**, 20983–20998.

Roelofs, G. J. and Lelieveld, J. 1997. Model study of the influence of cross-tropopause O_3 transports on tropospheric O_3 levels. *Tellus* **49B**, 38–55.

Savoie, D. L., Prospero, J. M. Larsen, R. J. Huang, F., Isaguirre, M., Huang, T., Snowdon, T. H., Custals, L. and Sanderson, C. G. 1993. Nitrogen and sulfur species in Antarctic aerosols at Mawson, Palmer Station, and marsh (King George Island). *J. Atmos. Chem.* **17**, 95–122.

Savoie, D. L., Prospero, J. M., Arimoto, R. and Duce, R. A. 1994. Non-sea-salt sulfate and methanesulfonate at American Samoa. *J. Geophys. Res.* **99**, 3587–3596.

Schwartz, S. E. 1986. Mass transport considerations pertinent to aqueous phase reactions of gases in liquid water clouds. In: *Multiphase atmospheric chemistry* (ed. W. Jaeschke). Springer Verlag, Berlin, pp. 415–471.

Schwartz, S. E. 1988. Mass transport limitation to the rate of in-cloud oxidation of SO_2: re-examination in the light of new data. *Atmos. Environ.* **22**, 2491–2499.

Scott, B. C. 1978. Parameterization of sulfate removal by precipitation. *J. Appl. Meteor.* **17**, 1375–1389.

Shaw, R. W. and Paur, R. J. 1983. Measurements of sulfur in gases and particles during sixteen months in the Ohio River Valley. *Atmos. Environ.* **17**, 1431–1438.

Spiro, P. A., Jacob, D. J. and Logan, J. A. 1992. Global inventory of sulfur emissions with $1^\circ \times 1^\circ$ resolution. *J. Geophys. Res.* **97**, 6023–6036.

Sundqvist, H. 1978. A parameterization scheme for non-convective condensation including prediction of cloud water content. *Quart. J. Roy. Meteor. Soc.* **104**, 677–690.

Tiedtke, M. 1989. A comprehensive mass flux scheme for cumulus parametrization in large-scale models. *Mon. Wea. Rev.* **117**, 1779–1800.

Twomey, S. 1974. Pollution and the planetary albedo. *Atmos. Environ.* **8**, 1251–1256.